Multiphase Ti_xO_y nanoparticles by pulsed laser ablation of titanium in supercritical CO_2

Amandeep Singh[a], Turkka Salminen[b], Mari Honkanen[b], Jorma Vihinen[c], Leo Hyvärinen[a], Erkki Levänen[a]

[a] Materials Science, Faculty of Engineering and Natural Sciences, Tampere University, P. O. Box 589, FIN 33101 Tampere, Finland

[b] Tampere Microscopy Center, Tampere University, P. O. Box 692, FIN 33101 Tampere, Finland

[c] Faculty of Engineering and Natural Sciences, Tampere University, P. O. Box 589, FIN 33101 Tampere, Finland

Author details:

Amandeep Singh : amandeep.singh@tut.fi

Turkka Salminen : turkka.salminen@tut.fi

Mari Honkanen : mari.honkanen@tut.fi

Jorma Vihinen : jorma.vihinen@tut.fi

Leo Hyvärinen : leo.hyvarinen@tut.fi

Erkki Levänen : erkki.levanen@tut.fi

Corresponding author: Amandeep Singh, Email: amandeep.singh@tut.fi

Abstract

In this paper, we demonstrate pulsed laser ablation (PLA) in supercritical CO_2 ($scCO_2$) as a promising method to synthesize multiphase Ti_xO_y nanoparticles from a titanium target. These results are compared against PLA of titanium in H_2O. By means of transmission electron microscopy, we observed spherical-shaped, well-dispersed non-agglomerate crystalline nanoparticles by PLA in $scCO_2$ while PLA in H_2O produced spherical-shaped as well as randomly shaped nanoparticles that joined to form web-like networks. Raman spectroscopy and x-ray diffraction showed nanoparticles synthesized in $scCO_2$ consisted of anatase-TiO_2, Ti_2O_3 and $TiO_{0.89}$ while nanoparticles synthesized in H_2O were mainly rutile-TiO_2, with possibility of presence of brookite-TiO_2. This indicates PLA in $scCO_2$ favours formation of metastable phases (anatase-TiO_2, Ti_2O_3 and $TiO_{0.89}$) while PLA in H_2O results in mostly stable phase (rutile-TiO_2).

Keywords: pulsed laser ablation, supercritical fluids, multiphase titanium oxides, non-stoichiometric compounds, metastable phases

1. Introduction

Titanium dioxide (TiO_2) has been a material of great interest in the scientific community as well as industry after its excellent photocatalytic properties were reported by Fujushima and Honda in 1972 [1]. It is now one of the most commonly used photocatalysts with numerous applications such as dye-sensitized solar cells [2], lithium ion batteries [3],water purification [4], and air purification [5]. TiO_2 has a band gap at approximately 3 eV, and thus requires blue or UV light to be active. There have been significant efforts to increase the absorption in the visible range by doping TiO_2 with non-metals (such as N, C) [6,7] and transition metals (such as Co, Rh, V, Fe, Cr, and Mn) [8]. Thakur et al. [9,10] reported production of nanomaterials of dopant free multiphase titanium oxides with increased absorption in vis-NIR region and average band gap of 2.39 eV. This behaviour of enhanced absorption spectrum of these nanomaterials was reportedly due to (i) presence of multiple titanium

oxide phases absorbing at different wavelengths, (ii) synthesized by a "unique fusion of plume formation and vapour condensation mechanism", and (iii) brought about by "interaction of ultra-short laser pulses and titanium substrate" using femtosecond laser ablation [10].

Amongst the nanoparticle synthesis methods, as evident from the increase in the publications in last decade by a factor of 15 [11], pulsed laser ablation in liquids (PLAL) has been extensively explored as a simple, versatile and green method [12,13]. Significant efforts have been made specially to understand plasma and cavitation dynamics in PLAL [14–16]. A shortcoming of this method has been low nanoparticle productivity, however, the latest demonstrations have shown production rates of up to 4 g/h [17] for Au, Ag, Ti, Cu, Al and Pt. With the production of nanoparticles of metals, ceramics, alloys, and semi-conductors, PLAL has been demonstrated to be a promising method for production of variety of nanoparticles [18,19].

In PLAL, the liquid surrounding the target has a significant role on the morphology, structure and phase of the synthesized nanoparticles [13]. Kuwahara et al. reported that during PLA of copper in pressurized CO_2, the ablation efficiency was several tens of times higher at elevated pressure [20]. In supercritical fluids, such as supercritical CO_2 ($scCO_2$), the PLA-induced plasma has been reported to be dense consisting of highly active species, allowing the synthesis of exotic nanomaterials [21]. As a typical supercritical fluid, $scCO_2$, it is possible to change its solvent power just by changing the temperature and pressure. Owing to its zero surface tension, it penetrates and leaves nanostructures unharmed. Additionally, particle synthesis with $scCO_2$ is a green process because CO_2 is non-toxic, rather inert, and recyclable in process and owing to its low critical point (7.4 MPa, 31.1 °C) [22], it is a low energy process especially compared to supercritical H_2O (22.1 MPa, 374 °C) [23]. Combination of plasma and supercritical fluids is sometimes advantageous also because of the synergic effect of highly reactive plasma species and superior transport properties of supercritical fluids [24]. Saitow et al. first reported synthesis of silicon nanoclusters [25], as well as, gold nanospheres and nanonecklaces [26] by PLA in $scCO_2$. Nakahara et al. demonstrated PLA in $scCO_2$ as

a promising method for synthesizing higher diamondoids, that are typically difficult to synthesize [27].

In our study, a titanium target was ablated in $scCO_2$ at 10 MPa and 50 °C using a 250 ns 1064 nm pulsed fiber laser at 101 kHz. To the best of our knowledge, this is the first study that demonstrates production of multiphase Ti_xO_y nanoparticles from titanium by PLA in $scCO_2$. The synthesized nanoparticles were studied by transmission electron microscope (TEM), x-ray diffraction (XRD), and Raman spectroscopy. By discussing the key results from (i) TEM, XRD and Raman for the nanoparticles and their phases formed from titanium by PLA in $scCO_2$, as well as (ii) their comparison with similar analysis from PLA of titanium in H_2O, this study demonstrates the potential of PLA in $scCO_2$ for synthesis of well-dispersed metastable multiphase nanomaterials without the use of liquid.

2. Experimental

2.1. Materials

A titanium sheet (99.99% pure), obtained from Goodfellow Cambridge Ltd, 3.2 mm thick and 50 x 50 mm, was cut into 15 x 15 mm sized target for the experiment. Carbon dioxide (≥ 99.8 % pure with O_2 ≤ 20 ppm, H_2O ≤ 100 ppm) was obtained from Oy AGA Ab.

2.2. Pulsed laser ablation in $scCO_2$ and H_2O: Setup and nanoparticle synthesis

The schematic in Figure 1 shows the experimental setup for PLA in $scCO_2$. The experimental set-up consisted of a 70W fiber laser (λ = 1064 nm) with a pulse duration of 250 ns and a repetition rate of 101 kHz. An 80 mm F-theta lens was used to focus the laser beam on the titanium target fixed inside the reaction chamber. The target was fixed using two neodymium magnets on a magnetic steel plate attached to the target holder and placed inside the chamber so that laser irradiates the target surface perpendicularly. The laser irradiated the titanium target for a 30-minute ablation period. The PLA in $scCO_2$ experiment was performed using a Thar Technologies Inc. RESS 250 system (Pittsburg, USA). The reaction chamber, made of 316SS steel, was suitable for pressures up to 60 MPa and

temperatures up to 150 °C. It consisted of heating rods built into the walls and two sapphire windows, one of which was used to introduce the laser pulses into the chamber. There was no cooling system installed with the high-pressure chamber. The PC-controlled automatic back-pressure regulator (ABPR) meticulously governed the depressurization rate of the CO_2 after the ablation process ended. BPR was used only to depressurize at the end of ablation process, so not to avoid pressure increase. CO_2 (gas) was flushed through the reaction chamber prior to ablation in order to reduce the amount of ambient atmospheric gases inside the chamber, in particular to alleviate the effects of O_2 and N_2. CO_2 was pumped into the chamber using a high-pressure piston-pump at a constant rate of 20g/min until the pressure stabilized at 10 MPa. The temperature of the reaction chamber was set to 50 °C. After the chamber pressure and temperature stabilized at 10 MPa and 50 °C respectively, laser beam scanned an area of 6 x 6 mm at a scanning rate of 2 m/s. After 30 minutes of laser ablation followed by depressurisation, the nanoparticles were collected from the chamber as a powder. The pressure and temperature sensors had an accuracy of 0.05 MPa and 1.1 °C respectively, as guaranteed by the supplier of the CO_2 system. The pressure sensor was just before the inlet valve of BPR while the temperature sensor was fitted inside the vessel. As the end of 30 minutes ablation, the pressure and temperature inside the chamber soared to 10.7 MPa and 59.4 °C respectively.

For PLA in H_2O, the schematic and set-up of equipment is explained in our previous publication [28]. However, the laser and its parameters used were same as in the aforementioned PLA in $scCO_2$ experiment and ablation time was 30 minutes. The water film thickness above the target was 4 mm. The loss in laser transmission was measured to be same for 13 mm thick sapphire window (PLA in $scCO_2$) and 4 mm thick water film above target (PLA in H_2O). After the experiment, the nanoparticles were collected in the form of nanoparticle suspension.

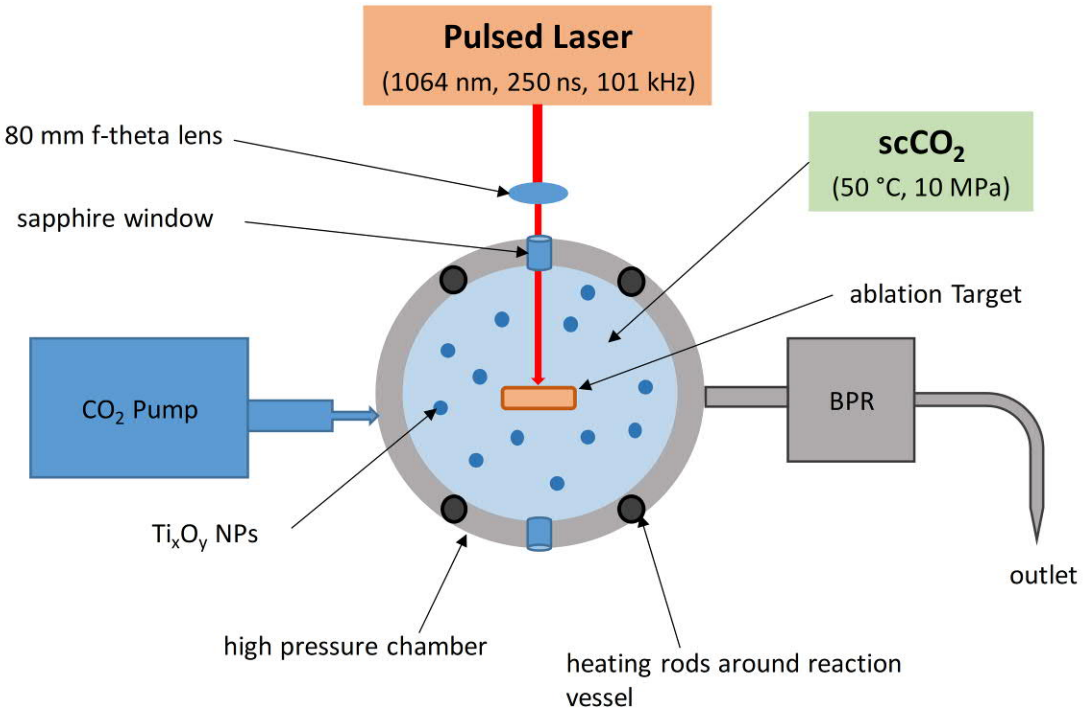

Figure 1 Schematic of PLA in $scCO_2$

2.3. Characterization methods

Jeol JEM-2010 TEM was used for imaging the nanoparticles to characterize the shape and size of nanoparticles. A high resolution TEM (Jeol, JEM-2200FS HRTEM) was used for high resolution imaging of nanoparticles. The TEM samples for nanoparticles obtained from PLA in $scCO_2$ were prepared by directly touching the TEM copper grids with a holey carbon film on dry nanoparticles from reaction chamber. TEM samples for nanoparticle suspensions from PLA in H_2O were made by dropping the suspension on copper grid with holey carbon film and allowing them to dry. Selected area electron diffraction (SAED) patterns were also obtained from the same TEM samples to study the crystallinity of samples.

XRD measurements were performed on a Panalytical Empyrean Multipurpose Diffractometer with a Cu Kα x-ray source (λ = 0.15418 nm) and a solid-state pixel detector, PIXcel3D, which measured the scattered intensities as a function of scattering angle (2θ). The x-ray generator was powered at 45 kV and 40 mA. For XRD measurements, the scan range was 20.00°-80.95° with a 0.05° step size. It used a soller slit with 0.04 radian opening. The phase identification of the peaks in the XRD pattern was

performed with Panalytical HighScore Plus software (version 3.0.5) from the database PDF-4+ of the International Centre for Diffraction data (Database version 4.1065). For further phase analysis, the Raman spectra were measured using Renishaw inVia Qontor Raman microscope. A 532 nm wavelength laser was used for excitation. For both XRD and Raman, the sample was as-deposited nanoparticle powders (from PLA in $scCO_2$) on the non-ablated part of the target. So, we can expect high peaks for titanium metal in the XRD pattern, however, not in the Raman plot since metals are not Raman active. The nanoparticle suspension from PLA in H_2O was dried to obtain powder of nanoparticles upon which XRD and Raman was performed.

3. Results and discussion

3.1. Comparative TEM analysis for PLA in $scCO_2$ and PLA in H_2O:

Figure 2a and 2b show the TEM micrographs for nanoparticles synthesized by PLA of titanium in $scCO_2$. The TEM images show uniformly dispersed spherical nanoparticles (Fig. 2a). The formation of round nanoparticles with PLA is well reported and is attributed to the diffusion of hot surface atoms on nanoparticles as well as melting of already synthesized nanoparticles because of laser processing in order to decrease interfacial energy [10]. In the SAED pattern (Fig. 2a inset), crystalline rings were observed indicating the presence of mainly nanocrystalline particles. It is noteworthy to mention we did not observe any large nanospheres in this study such as the ones reported in a study by Saitow et al. where they observed 400 nm large gold nanospheres as a result of PLA in $scCO_2$ at relatively higher CO_2 densities (1.7 g/cm^3) [26]. In our study, the CO_2 density varies between 0.34 – 0.38 g/cm^3 for pressures and temperatures mentioned in the experimental section. At smaller densities, PLA in supercritical fluids such as CO_2 and trifluoromethane (CHF_3) leads to formation of nanoparticles few tens of nanometers in diameter, while at higher densities, it leads to formation of large nanospheres and nanonecklaces [26,29].

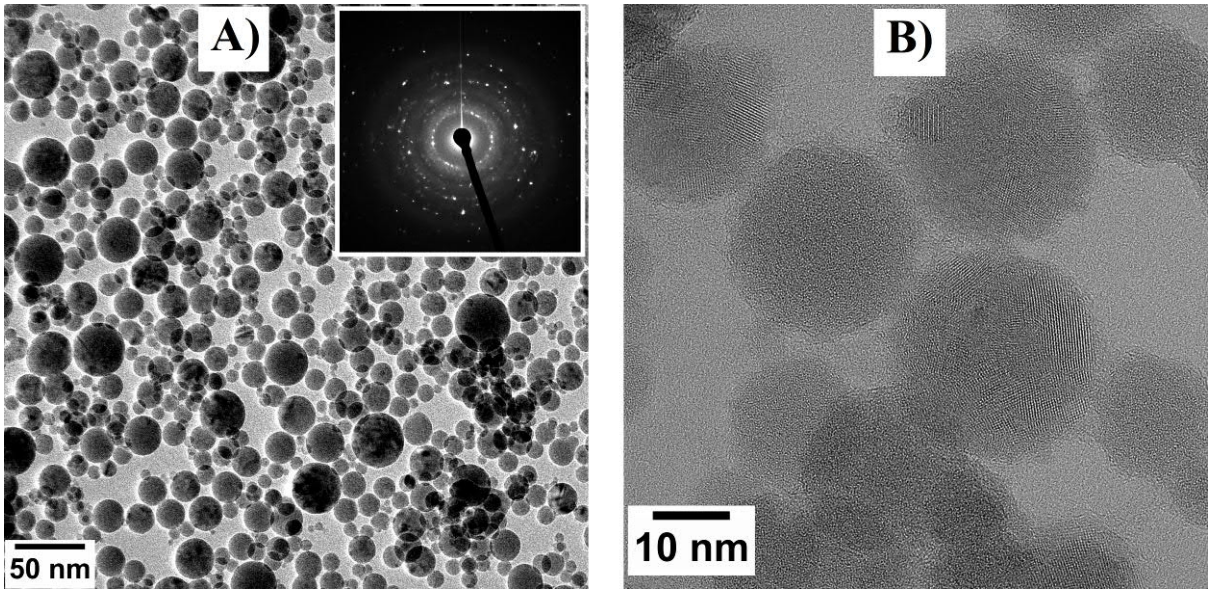

Figure 2 TEM micrographs (a and b) and SAED pattern (as inset in a) from nanoparticles synthesized by PLA in $scCO_2$

Figure 3a and 3b show the TEM micrographs of the nanoparticles synthesized by PLA of titanium in H_2O. In the TEM images, round nanoparticles were observed to form web-like structures. Others have reported formation of similar web-like structure upon PLA in H_2O [30]. In addition, with higher magnification (Fig. 3b), randomly shaped nanoparticles were observed that joined with each other as well as with the spherical bigger nanoparticle indicating agglomeration. SAED pattern taken from this region (Fig. 3a inset) showed crystalline rings and spots and maybe also diffuse rings, indicating presence of crystalline and possibly some amorphous forms.

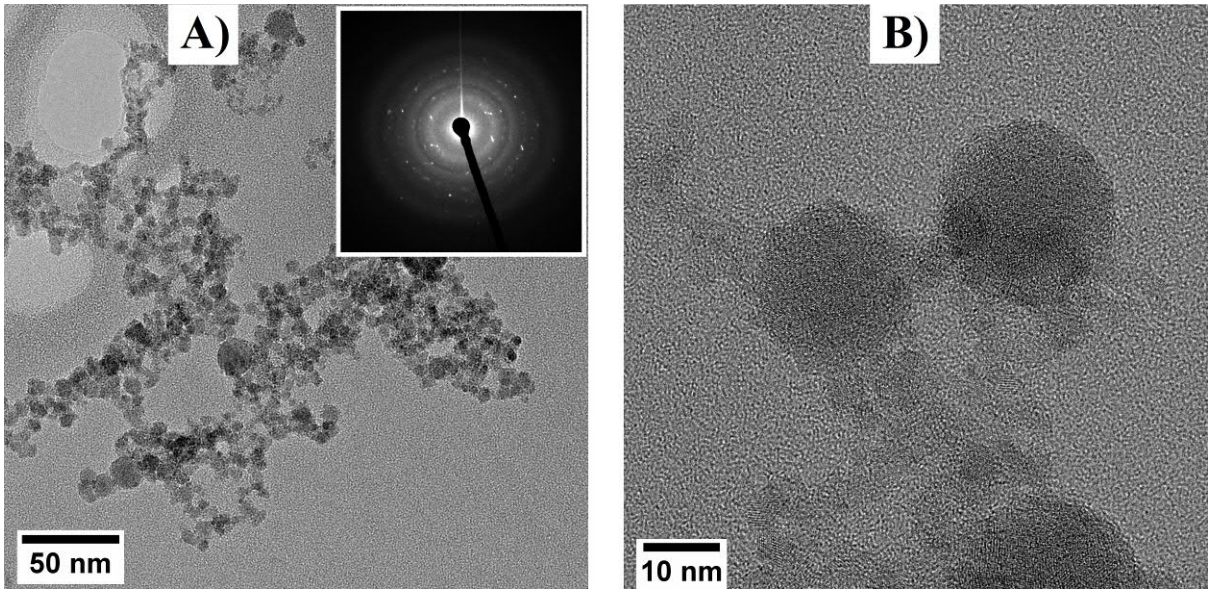

Figure 3 TEM micrographs (a and b) and SAED pattern (as inset in a) from nanoparticles synthesized by PLA in H_2O.

In PLA in $scCO_2$, the nanoparticles were uniformly dispersed and non-agglomerated. This may occur due to the polar nature of synthesized nanoparticles surrounded by $scCO_2$, which is non-polar and has zero surface tension. For PLA in $scCO_2$ (Fig. 2a and 2b), randomly shaped nanoparticles observed for PLA in H_2O (Fig. 3a and 3b), were not observed. In case of PLA in $scCO_2$, in theory, the electrical double layer, that usually surrounds the nanoparticles in aqueous medium, should be absent. In addition, no hydrogen is involved in the process, so the possibility of firstly hydrogen bonding of the particles and secondly presence of OH^-, H_3O^+, and H^+ ions can be eliminated due to which no agglomeration was observed. This suggests PLA in $scCO_2$ in a promising method for synthesis of well-dispersed non-agglomerated spherical-shaped nanoparticles via a dry process. Later after the process is finished, it is however possible that H_2O (moisture) adsorbs on the nanoparticles when exposed to the ambient environment outside the reaction chamber causing some agglomeration.

3.2. Comparative Phase analysis – Raman and XRD of the nanoparticles

Raman measurements from the nanoparticle powder on the target surface (Fig. 4a) synthesized by PLA in $scCO_2$ indicated presence of mainly anatase –TiO_2 with the possibility of minor amounts of titanium(III) oxide (Ti_2O_3). The broad features might belong to smaller peaks of anatase, titanium(III) oxide (Ti_2O_3) or other titanium oxides. Raman analysis did not show peaks at 222, 420 or 605 cm^{-1} corresponding to TiC indicating absence of titanium carbides. The Raman spectra for nanoparticles synthesized by PLA in H_2O (Fig.4b) showed two prominent peaks at 440 cm^{-1} and 610 cm^{-1} indicating presence of mostly rutile-TiO_2. The peak at around 150 cm^{-1} suggests presence of anatase, brookite or a combination of both. In addition to those, the broad pedestal up to 900 cm^{-1} may signify presence of disordered or amorphous material.

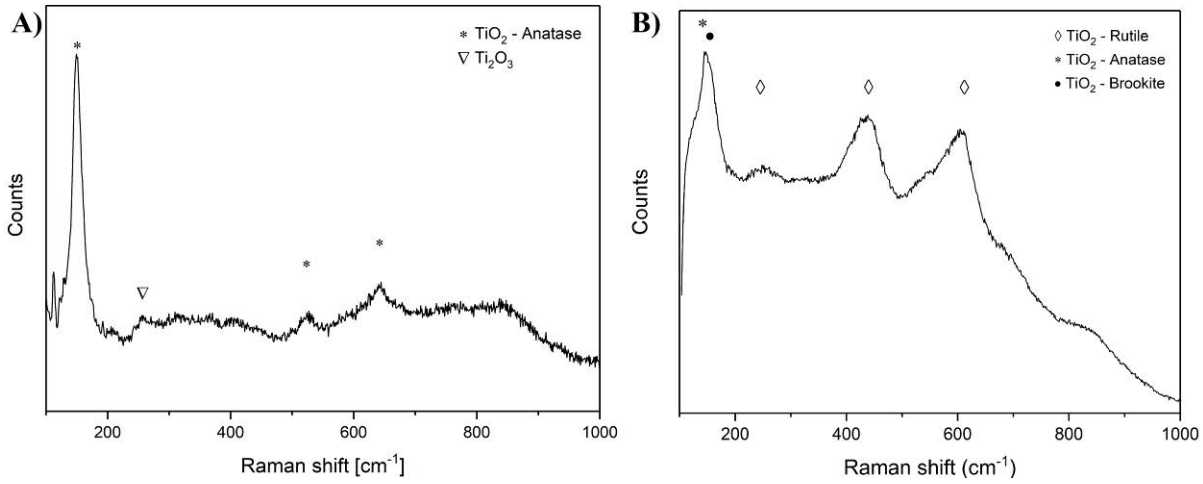

Figure 4 Raman spectra of nanoparticles formed by (a) PLA in scCO2 and (b) PLA in H2O

XRD results for PLA in $scCO_2$ synthesized nanoparticles (Fig. 5a) corroborated the presence of anatase-TiO_2 and titanium(III) oxide (Ti_2O_3). Additionally, XRD, indicated presence of a non-stoichiometric oxide of titanium - $TiO_{0.89}$, which is a high-temperature phase. XRD from the samples prepared in H_2O (Fig. 5b) strongly indicate that the material is mostly rutile-TiO2. There were four prominent peaks observed for rutile-TiO_2 at 27.4, 36.0, 41.2, and 54.3 degrees. The broadened peak at 54.3 also has a shoulder due to another rutile peak at 56.6 degrees. The peaks in XRD pattern are broadened due to small size of nanoparticles. The small peak at 25.3 degrees may correspond to brookite-TiO_2. The broadened small peaks between 62 and 70 degrees correspond to rutile-TiO_2 or a combination of rutile-TiO_2 and brookite-TiO_2 phase. This agrees with the Raman results that rutile was the main phase and along with trace amounts of brookite. Interestingly, from the Raman and XRD investigation, we observe formation of mostly metastable phases in PLA in $scCO_2$ – anatase TiO_2, Ti_2O_3 and $Ti_{O.89}$, while PLA in H_2O resulted in mostly stable phase – rutile TiO_2.

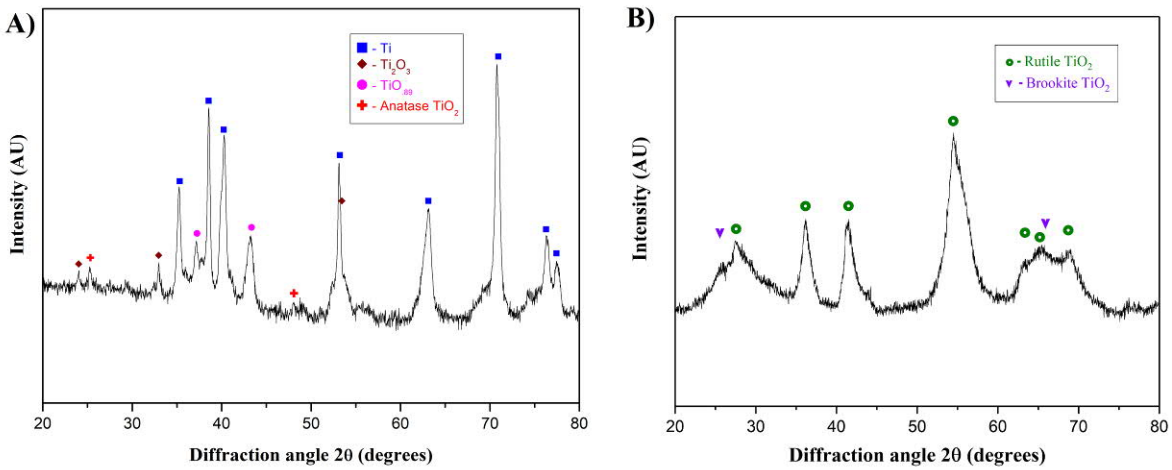

Figure 5 XRD pattern of nanoparticles formed by (a) PLA in scCO2 and (b) PLA in H2O

3.3. Comparative analysis of source of oxidation

CO_2 has low reactivity; however, in the presence of high-temperature high-pressure plasma, its dissociation forms O^-/O_2, with which the ablated plasma species can react. The minimum energy path for the dissociation of CO_2 leads to CO and O^-, which can further combine to form CO_2 and O_2. Under extreme conditions, CO_2 can dissociate directly to carbon and molecular oxygen through vacuum ultraviolet photodissociation [31] or dissociative electron attachment [32]. For PLA in H_2O, the laser ablated materials react with oxygen [33], that is either dissolved in water [34] or bound to water molecule which can be made available by plasma-induced water splitting [35].

According to Ellingham diagram [36], CO_2 is more oxidizing than H_2O at temperatures below 1000 K. However, in our experiments the samples prepared in H_2O were completely oxidised which can be explained if the oxygen, that is dissolved in the water, is responsible for the oxidation. Thorough thermodynamic analysis of this process is beyond the scope of this study.

Although carbide compounds were not observed in this study, PLA in $scCO_2$ at higher CO_2 pressures will make an interesting future scope of work to reveal the consequential effect of variation in plasma and cavitation bubble dynamics (or dynamics of the bubble-like hollow) on nanoparticle size, morphology, and phase.

4. Conclusion

In summary, production of well-dispersed non-agglomerated Ti_xO_y nanoparticles by PLA of titanium in $scCO_2$ was successfully demonstrated via green synthesis using only supercritical CO_2 as the solvent. The results from this technique were compared against results from PLA of titanium in H_2O. The nanoparticles were studied by TEM, Raman microscopy and XRD. TEM showed spherical-shaped, well-dispersed crystalline nanoparticles. By PLA in $scCO_2$, we also report absence of any web-like networks or unwanted randomly shaped nanoparticles that were observed for nanoparticles synthesized in PLA in H_2O. Raman and XRD indicated nanoparticles synthesized by PLA in $scCO_2$ were anatase-TiO_2, Ti_2O_3, and $TiO_{0.89}$. For nanoparticles synthesized by PLA in H_2O, Raman and XRD indicated presence of mostly rutile-TiO_2 along with trace amounts of brookite-TiO_2. This suggests that PLA in $scCO_2$ favours formation of metastable phases and forms with crystallographic defects and vacancies such as $TiO_{0.89}$, while PLA in H_2O favours formation of mostly stable phase such as rutile-TiO_2.

Acknowledgements:

This work was supported by NanoStencil - Proposal number 767285, which is a H2020 FET-Open project funded by the EU. We acknowledge the provision of facilities and technical support by Aalto University at OtaNano - Nanomicroscopy Center (Aalto-NMC). We acknowledge senior scientist Dr. Hua Jiang for performing high resolution TEM studies at Aalto University. This work made use of Tampere Microscopy Center facilities at Tampere University.

Declaration

The authors declare no conflict of interest.

References

[1] A. Fujishima, K. Honda, Electrochemical Photolysis of Water at a Semiconductor Electrode, Nature. 238 (1972) 37–38. doi:10.1038/238037a0.

[2] K. Tennakone, A.R. Kumarasinghe, P.M. Sirimanne, G.R.R.A. Kumara, Deposition of thin

polycrystalline films of cuprous thiocyanate on conducting glass and photoelectrochemical dye-sensitization, Thin Solid Films. 261 (1995) 307–310. doi:10.1016/S0040-6090(95)06523-7.

[3] I. Exnar, L. Kavan, S.Y. Huang, M. Grätzel, Novel 2 V rocking-chair lithium battery based on nano-crystalline titanium dioxide, J. Power Sources. 68 (1997) 720–722. doi:10.1016/S0378-7753(96)02581-5.

[4] D. Friedmann, C. Mendive, D. Bahnemann, TiO2 for water treatment: Parameters affecting the kinetics and mechanisms of photocatalysis, Appl. Catal. B Environ. 99 (2010) 398–406. doi:10.1016/j.apcatb.2010.05.014.

[5] A. Fujishima, T.N. Rao, D. a. Tryk, Titanium dioxide photocatalysis, J. Photochem. Photobiol. C Photochem. Rev. 1 (2000) 1–21. doi:10.1016/S1389-5567(00)00002-2.

[6] C. Burda, Y. Lou, X. Chen, A.C.S. Samia, J. Stout, J.L. Gole, Enhanced Nitrogen Doping in TiO 2 Nanoparticles, Nano Lett. 3 (2003) 1049–1051. doi:10.1021/nl034332o.

[7] D. Chen, Z. Jiang, J. Geng, Q. Wang, D. Yang, Carbon and Nitrogen Co-doped TiO 2 with Enhanced Visible-Light Photocatalytic Activity, Ind. Eng. Chem. Res. 46 (2007) 2741–2746. doi:10.1021/ie061491k.

[8] B. Liu, H.M. Chen, C. Liu, S.C. Andrews, C. Hahn, P. Yang, Large-scale synthesis of transition-metal-doped TiO2 nanowires with controllable overpotential, J. Am. Chem. Soc. 135 (2013) 9995–9998. doi:10.1021/ja403761s.

[9] P. Thakur, B. Tan, K. Venkatakrishnan, Multi-phase functionalization of titanium for enhanced photon absorption in the vis-NIR region, Sci. Rep. 5 (2015) 15354. doi:10.1038/srep15354.

[10] P. Thakur, B. Tan, K. Venkatakrishnan, Multiphase titanium oxide nanomaterial for augmented vis-NIR photon absorption, Sol. Energy Mater. Sol. Cells. 152 (2016) 161–169. doi:10.1016/j.solmat.2016.03.037.

[11] S. Barcikowski, F. Devesa, K. Moldenhauer, Impact and structure of literature on nanoparticle generation by laser ablation in liquids, J. Nanoparticle Res. 11 (2009) 1883–1893. doi:10.1007/s11051-009-9765-0.

[12] D. Zhang, B. Gökce, S. Barcikowski, Laser Synthesis and Processing of Colloids: Fundamentals and Applications, Chem. Rev. 117 (2017) 3990–4103. doi:10.1021/acs.chemrev.6b00468.

[13] H. Zeng, X.-W. Du, S.C. Singh, S.A. Kulinich, S. Yang, J. He, W. Cai, Nanomaterials via Laser Ablation/Irradiation in Liquid: A Review, Adv. Funct. Mater. 22 (2012) 1333–1353. doi:10.1002/adfm.201102295.

[14] J. Lam, D. Amans, F. Chaput, M. Diouf, G. Ledoux, N. Mary, K. Masenelli-Varlot, V. Motto-Ros, C. Dujardin, γ-Al2O3 nanoparticles synthesised by pulsed laser ablation in liquids: a plasma analysis, Phys. Chem. Chem. Phys. 16 (2014) 963–973. doi:10.1039/C3CP53748J.

[15] R. Tanabe, T.T.P. Nguyen, T. Sugiura, Y. Ito, Bubble dynamics in metal nanoparticle formation by laser ablation in liquid studied through high-speed laser stroboscopic videography, Appl. Surf. Sci. 351 (2015) 327–331. doi:10.1016/j.apsusc.2015.05.030.

[16] J. Lam, J. Lombard, C. Dujardin, G. Ledoux, S. Merabia, D. Amans, Dynamical study of bubble expansion following laser ablation in liquids, Appl. Phys. Lett. 108 (2016) 074104. doi:10.1063/1.4942389.

[17] R. Streubel, S. Barcikowski, B. Gökce, Continuous multigram nanoparticle synthesis by high-power, high-repetition-rate ultrafast laser ablation in liquids, Opt. Lett. 41 (2016) 1486. doi:10.1364/OL.41.001486.

[18] Z. Yan, D.B. Chrisey, Pulsed laser ablation in liquid for micro-/nanostructure generation, J. Photochem. Photobiol. C Photochem. Rev. 13 (2012) 204–223. doi:10.1016/j.jphotochemrev.2012.04.004.

[19] V. Amendola, M. Meneghetti, What controls the composition and the structure of nanomaterials generated by laser ablation in liquid solution?, Phys. Chem. Chem. Phys. 15 (2013) 3027–3046. doi:10.1039/C2CP42895D.

[20] Y. Kuwahara, T. Saito, M. Haba, T. Iwanaga, M. Sasaki, M. Goto, Nanosecond Pulsed Laser Ablation of Copper in Supercritical Carbon Dioxide, Jpn. J. Appl. Phys. 48 (2009) 040207. doi:10.1143/JJAP.48.040207.

[21] K. Urabe, T. Kato, S. Stauss, S. Himeno, S. Kato, H. Muneoka, M. Baba, T. Suemoto, K. Terashima, Dynamics of pulsed laser ablation in high-density carbon dioxide including supercritical fluid state, J. Appl. Phys. 114 (2013) 143303. doi:10.1063/1.4824538.

[22] W. Leitner, Designed to dissolve, Nature. 405 (2000) 129–130. doi:10.1038/35012181.

[23] N. Takada, S. Machmudah, Characteristics of optical emission intensities and bubblelike phenomena induced by laser ablation in supercritical fluids, Jpn. J. Appl. Phys. 010213 (2014). http://iopscience.iop.org/1347-4065/53/1/010213 (accessed November 19, 2014).

[24] T. Tomai, K. Katahira, H. Kubo, Y. Shimizu, T. Sasaki, N. Koshizaki, K. Terashima, Carbon materials syntheses using dielectric barrier discharge microplasma in supercritical carbon dioxide environments, J. Supercrit. Fluids. 41 (2007) 404–411. doi:10.1016/j.supflu.2006.12.003.

[25] K. Saitow, Silicon Nanoclusters Selectively Generated by Laser Ablation in Supercritical Fluid, J. Phys. Chem. B. 109 (2005) 3731–3733. doi:10.1021/jp0442551.

[26] K. Saitow, T. Yamamura, T. Minami, Gold nanospheres and nanonecklaces generated by laser ablation in supercritical fluid, J. Phys. Chem. C. 112 (2008) 18340–18349. http://pubs.acs.org/doi/abs/10.1021/jp805978g.

[27] S. Nakahara, S. Stauss, T. Kato, T. Sasaki, K. Terashima, Synthesis of higher diamondoids by pulsed laser ablation plasmas in supercritical CO2, J. Appl. Phys. 109 (2011) 123304 (1-8). doi:10.1063/1.3599887.

[28] A. Singh, J. Vihinen, E. Frankberg, L. Hyvärinen, M. Honkanen, E. Levänen, Pulsed Laser Ablation-Induced Green Synthesis of TiO2 Nanoparticles and Application of Novel Small Angle X-Ray Scattering Technique for Nanoparticle Size and Size Distribution Analysis, Nanoscale Res. Lett. 11 (2016) 447. doi:10.1186/s11671-016-1608-1.

[29] K.I. Saitow, Y. Okamoto, Y.F. Yano, Fractal of gold nanoparticles controlled by ambient dielectricity: Synthesis by laser ablation as a function of permittivity, J. Phys. Chem. C. 116 (2012) 17252–17258. doi:10.1021/jp304109h.

[30] G. Ledoux, D. Amans, C. Dujardin, K. Masenelli-Varlot, Facile and rapid synthesis of highly luminescent nanoparticles via pulsed laser ablation in liquid, Nanotechnology. 20 (2009) 445605. doi:10.1088/0957-4484/20/44/445605.

[31] Z. Lu, Y.C. Chang, Q.-Z. Yin, C.Y. Ng, W.M. Jackson, Evidence for direct molecular oxygen production in CO2 photodissociation, Science (80-.). 346 (2014) 61–64. doi:10.1126/science.1257156.

[32] X.-D. Wang, X.-F. Gao, C.-J. Xuan, S.X. Tian, Dissociative electron attachment to CO2 produces molecular oxygen, Nat. Chem. 8 (2016) 258–263. doi:10.1038/nchem.2427.

[33] J. Lam, D. Amans, C. Dujardin, G. Ledoux, A.-R. Allouche, Atomistic Mechanisms for the Nucleation of Aluminum Oxide Nanoparticles, J. Phys. Chem. A. 119 (2015) 8944–8949. doi:10.1021/acs.jpca.5b05829.

[34] G. Marzun, H. Bönnemann, C. Lehmann, B. Spliethoff, C. Weidenthaler, S. Barcikowski, Role of Dissolved and Molecular Oxygen on Cu and PtCu Alloy Particle Structure during Laser Ablation Synthesis in Liquids, ChemPhysChem. 18 (2017) 1175–1184. doi:10.1002/cphc.201601315.

[35] M. Kalus, N. Bärsch, R. Streubel, E. Gökce, S. Barcikowski, B. Gökce, How persistent microbubbles shield nanoparticle productivity in laser synthesis of colloids – quantification of their volume, dwell dynamics, and gas composition, Phys. Chem. Chem. Phys. 19 (2017) 7112–7123. doi:10.1039/C6CP07011F.

[36] D.R. Gaskell, Introduction to the Thermodynamics of Materials, Taylor and Francis, London, 1995.